Research Article

Enhanced photocatalytic reduction of toxic Cr(VI) with Cu modified ZnO nanoparticles in presence of EDTA under UV illumination

Jahida Binte Islam[1] · Mai Furukawa[1] · Ikki Tateishi[2] · Shiho Kawakami[1] · Hideyuki Katsumata[1] · Satoshi Kaneco[1,2]

Abstract

In this study, the photocatalytic reduction of Cr(VI) to Cr(III) in aqueous solution using 1 wt% Cu/ZnO photocatalyst in presence of ethylenediaminetetraacetic acid (EDTA) under UV irradiation was investigated. The photocatalytic Cr(VI) reduction with ZnO under UV irradiation was significantly low. A fast Cr(VI) reduction with ZnO was recorded in presence of EDTA. Results demonstrated that the rate constant raised from 1.6×10^{-2} to 7.5×10^{-2} min^{-1} with 20 ppm EDTA addition. The optimum reduction (90%) was observed within 30 min at pH 3. The reduction efficiency of Cr(VI) was evidently increased from 6% to 99%, with increasing ZnO dosages up to 40 mg. The role of co-catalysts such as Au, Ag, Cu and NiO was also studied. The addition of Cu ion remarkably accelerated the reduction of Cr(VI), compared with ZnO/EDTA system alone. The Cu motivated ZnO/EDTA system completed the 99% reduction within only 30 min. The Cu ions were reduced to metallic copper and Cu_2O by conduction band electrons of ZnO. The electron–hole recombination was gently declined by the shallow electron trapping of Cu. On the other hand, EDTA could be performed in two ways by forming Cr(III)-complex and separating Cr(III) from ZnO surface and by consuming valence band holes. The Cu modified ZnO photocatalyst was characterized by N_2 adsorption- desorption isotherm, TEM, EDX, XPS, DRS and PL spectra. We evaluated the influence of pH, photocatalyst dosage, initial concentration of EDTA and initial concentration of Cu^{2+} ion (Cu doping amount) on photocatalytic reduction of Cr(VI). The pseudo first order kinetic reaction was confirmed for this reduction process. Herein, a probable mechanism of this photocatalytic reduction process was also presented.

Keywords Photocatalytic reduction · ZnO nanoparticles · EDTA · Electron–hole recombination · Cu modification

1 Introduction

The 21st most abundant element of the earth's crust is chromium. Although chromium naturally occur as metal, it is conventionally admitted as a toxic element. This notorious chromium level has been increased in surface water with the development of urbanization and industrialization. Lather tanning, electroplating, metal corrosion inhibition, dye, pigment and alloy manufacturing industries release huge amount of chromium into nature every day [1, 2]. Between the two common oxidized forms such as hexavalent chromium (Cr(VI)) and trivalent chromium (Cr(III)), the Cr(III) is less pernicious than the Cr(VI) [3].The non-biodegradability and high mobility of Cr(VI)

in nature can present a mutagenic and carcinogenic risk for all living organisms [4]. On contrast, a trace amount of Cr(III) is required for human and animal health, since it is essential for sugar and lipid metabolism [5]. The World Health organization (WHO) firmly recommended that the maximum permissible level of Cr(VI) should be less than 50 µg/L^{-1} in drinking water [6]. Hence, the removal of toxic Cr(VI) from wastewater has been necessitated immensely. Electrocoagulation, microfiltration, adsorption, ion exchange, chemical precipitation, and etc. are generally applied to eliminate Cr(VI) from industrial waste water [7–11]. Nevertheless, these multifarious processes generally require a large instrumentation and huge amount of chemicals and organic additives, all of which markedly interrupt their practical use. Moreover, the production of secondary pollutants is another drawback of these traditional methods [12, 13]. Amid the most useful strategies, photocatalytic reduction using semiconductor-based photocatalyst overcomes these mentioned limitations impressively. Photocatalytic reduction technology manifests a high reduction efficiency and low energy consumption. The low cost and simple application make this process quite attractive to reduce hazardous Cr(VI) to benevolent Cr(III) [14]. Furthermore, photocatalysts can be recycled and reused repeatedly after completing photocatalytic reduction process [15].

Numerous semiconductor photocatalysts, for instance, TiO_2, ZnO, CdS and WO_3 have received great consideration for photocatalytic treatment of heavy metals, textile dyes and other toxic pollutants [16–19]. This photocatalytic method generally involves the migration of valence electrons to conduction band, when photocatalyst are irradiated under light having photons with more energy than bandgap of the photocatalyst. Migrated conduction band electrons can reduce the toxic heavy metal if the redox potential of reactant is more positive than the conduction band of photocatalyst [20]. ZnO is also an appealing semiconductor photocatalyst along TiO_2, since both have almost the same band gap (~ 3.20 eV) and chemically stable properties [21, 22]. According to some researchers, ZnO shows better photocatalytic activity than TiO_2 [23, 24]. The study demonstrated that ZnO nanoparticles can photoreduce toxic Cr(VI) efficiently to less toxic Cr(III). However, the application of ZnO powder during photoreduction of Cr(VI) still faces some limitations such as solubility below pH 3, poor dispersity and rapid combination of photoinduced electron–hole as well as narrow range of light response. Hence, it is essential to improve the photocatalytic activity of ZnO. The addition of sacrificial electron donors [25], composite formation such as ZnO/TiO$_2$, ZnO/CuS and ZnO/ZnFe$_2$O$_4$ [26, 27] or/and metal doping can modify the photocatalytic properties of ZnO [28, 29]. Recently, some common sacrificial electron donors, namely citric acid, EDTA, oxalic acid, formic acid and tartaric acid, have been tested on the reduction of Cr(VI) [3, 30]. Bao et al. explained it that EDTA gave the most positive effect on improving the Cr(VI) reduction compared with other sacrificial electron donors. Moreover, the number of carboxyl groups also controlled the reduction efficiency. Accordingly, EDTA enhanced Cr(VI) reduction more than the case with oxalate because oxalate readily oxidizes to CO_2 during the photocatalytic process, while EDTA produces several intermediates in route to its mineralization, which may also contribute to the synergistic effect [31]. In addition, Westin and Rasmuson reported that the presence of ethylenediaminetetraacetic acid (EDTA) can control the sizes and morphologies of the particles owing to the chelating effects of EDTA with metal ions of solution [32]. Therefore, Cr(VI)/EDTA mixed system has been grabbed immense attention to accelerate the heterogeneous photocatalytic Cr(VI) reduction [33].

Among different metallic candidates, copper (Cu) is a very promising material for photocatalysts modification. Copper is an inexpensive material comparing with other noble metals (gold, platinum and silver) recognized as very efficient co-catalysts of ZnO [34]. Furthermore, copper shows similar properties as gold and silver, due to occupying in the same group of the periodic table and its electronic configuration and the face centered cubic (FCC) structure of the atom's location. Under irradiation, copper ion forms complexes with organic acids and ultimately reduces to copper metal [35]. Moreover, Cu doping into ZnO can modify its electrical, optical and photocatalytic activity significantly [28]. Therefore, copper can be applied as potential co-catalyst with ZnO nanoparticles to enhance the photocatalytic behavior of ZnO nanoparticles. Even though the photocatalytic activities of ZnO nanoparticles have been examined for degradation various organic pollutants as well as heavy metals, to the best of our knowledge, the performance of Cu motivated ZnO semiconductor for Cr(VI) photo-reduction in presence of EDTA under UV illumination has not been investigated yet.

Therefore, the paper work aims to go a step forward in the perception of the key step to maximize the photocatalytic reduction of Cr(VI) with Cu motivated ZnO photocatalyst in presence of EDTA under UV irradiation.

2 Experimental

2.1 Chemicals and materials

ZnO nanopowder (surface area 15–25 m^{2}g^{-1}, particle size 50–70 nm) were purchased from SIGMA–ALDRICH Co. USA. One thousand ppm chromium (Cr^{6+}), 1000 ppm copper (Cu^{2+}) standard solution and 1,5-diphenylcarbazid

$(C_{13}H_{14}N_4O)$ powder were brought from Wako Pure Chemicals Industries Ltd., Osaka, Japan. EDTA–2Na and acetone (C_3H_6O) were obtained from Kishida Chemical Co. Ltd., Osaka, Japan. All chemical were used without further purification. NaOH (1.0 mol/L) and HNO_3 (1.0 mol/L) were used to adjust solution pH.

2.2 Photocatalytic run

Photocatalytic reduction of Cr(VI) was conducted in a 50 mL Pyrex vessel as reactor placing on magnetic stirrer. A black light (Toshiba Lighting & Technology Corp., 15 W) was positioned on the side of reactor as light source with a maximum emission of about 352 nm. The light intensity was determined by a digital UV intensity meter (USHIO, UIT–201) with a sensor (UV–365PD, 330 ~ 390 nm), and the value was 0.25 mW/cm^2. For this treatment, 40 mg ZnO photocatalyst was dispersed into 30 mL aqueous solution of hexavalent chromium (10 mg/L). Then, 40 ppm EDTA as a hole scavenger and 40 μL Cu^{2+} ion (1000 ppm) as co-catalyst were added into solution at room temperature. In dark, the sample was continuously stirred on magnetic stirrer for 30 min to achieve adsorption–desorption equilibrium of Cr(VI) on the surface of Cu modified ZnO. At specific interval, 1.5 mL aliquot was taken out and centrifuged at 1000 rpm for 15 min instantly to suppress nano powder from the solution. The concentration of Cr(VI) was determined by the Neslerization method using UV–VIS spectrophotometer at 540 nm.

2.3 Characterization

The specific surface area was determined by the Brunauer–Emmett–Teller N_2 adsorption- desorption isotherm measurement using BELSORP–mini II (BEL Japan). The morphology of ZnO and Cu/ZnO were observed by a transmission electron microscope (TEM; HITACHI S–4000, Japan). The elemental analysis of Cu/ZnO nanoparticles

has been prepared by energy dispersive X–ray spectroscopy (EDS). X–ray photoelectron Spectroscopy (XPS) measurement of Cu/ZnO photocatalyst was conducted on PHI Quantera SXM. To obtain band gap of photocatalyst, UV–VIS diffuse reflectance spectra (DRS) were recorded in the range of 200–870 nm on a UV spectrophotometer (V–750 SHIMAZU, Japan) equipped with an integrating sphere attachment, using $BaSO_4$ as reference. Photoluminescence spectra (PL) were recorded on a Fluorescence Spectrophotometer (RF–5300PC, SHIMAZU).

For the reusability of photocatalysts, 1 wt% Cu/ZnO was collected after each cycle by centrifugation. Then were washed with deionized water and ethanol. Then dried catalyst 1 wt% Cu/ZnO was used for next run. The further procedure for Cr(VI) reduction process was the same as mentioned above, except for the addition of Cu ion.

3 Result and discussion

3.1 Photocatalytic reduction of aqueous Cr(VI)

3.1.1 Influence of EDTA addition

The influence of EDTA addition on Cr(VI) removal was investigated using 0 ppm to 100 ppm EDTA with 10 ppm Cr(VI) as initial concentration. Result was shown in Fig. 1. It explained that 78% photocatalytic reduction of Cr(VI) was achieved with ZnO after 120 min in the absence of EDTA, while this percentage raised to 98.5 after adding 10 ppm to 100 ppm EDTA. The improvement may be due to the fact that organic additives containing EDTA become an effective electron donor, which captured positively charged holes (h^+) generated in valence band and more negatively charged electrons participated in the reduction of Cr(VI) simultaneously [36]. Consequently, reduction of Cr(VI) was accelerated. On contrary, Litter et al. [31] explained that the Cr(III) deposition onto photocatalyst

Fig. 1 Effect of EDTA addition on the photocatalytic reduction of Cr(VI) with ZnO (**a**); The plot of ln(C_0/C) versus irradiation time (**b**)
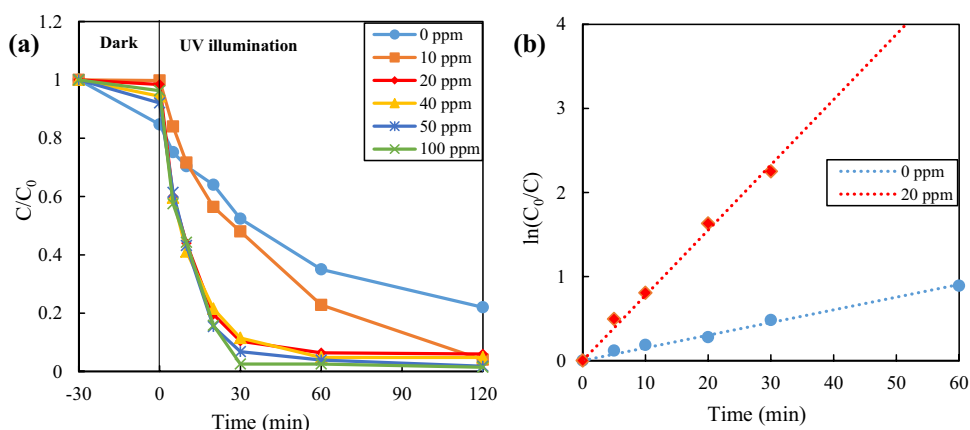
surface after reduction was inhibited due to the formation of Cr(III)-EDTA complex for the advanced photocatalytic activity of photocatalyst. Since the reduction rate of Cr(VI) over 20 to 100 ppm EDTA was almost the same, more than 20 ppm of EDTA was favorable for this experiment.

The photocatalytic reaction kinetics has been elucidated by Langmuir–Hinshewood (L–H) model explaining the relationship between initial concentration of Cr(VI) and reduction rate of Cr(VI). If the Cr(VI) concentration is very low, that is, $1 \gg K[Cr(VI)]$, the reduction rate will aid to pseudo-first-order kinetic law [25, 37].

$$r = \frac{d[Cr(VI)]}{dt} = kK[Cr(VI)] = k_{obs}[Cr(VI)]$$
$$-\ln\frac{[Cr(VI)]}{[Cr(VI)]_0} = k_{obs}t \quad (1)$$

where, $[Cr(VI)]_0$ is the initial Cr(VI) concentration, t is the irradiation time and k_{obs} is the pseudo-first-order rate constant (min^{-1}).

The kinetics of this photocatalytic reduction of Cr(VI) with ZnO in presence of 20 ppm of EDTA was explained in Fig. 1b where, $\ln(C_0/C)$ was plotted against irradiation time (t). The kinetic parameters such as the rate constant, correlation coefficient and substrate half-life were presented in Table 1. Table 1 demonstrated that rate constant increased from 1.6×10^{-2} to 7.5×10^{-2} min^{-1} with increasing the initial concentration from 0 to 20 ppm EDTA, respectively.

3.1.2 Influence of ZnO dosage

The reduction rate of Cr(VI) was affected by changing of ZnO dosages in presence of 100 ppm EDTA. As depicted in Fig. 2, the photocatalytic reduction of Cr(VI) was rapidly increased with increasing ZnO dosage from 10 to 50 mg. Briefly, it was seen that the reduction of Cr(VI) without ZnO was only 6% after 120 minutes, while 99% reduction was recorded with 40 mg of ZnO dosage under the same reduction condition. No significant result was shown with further accretion of the ZnO dosage. Since the adsorption sites on the ZnO photocatalyst can be increased due to large amount of photocatalyst dosage, hence, the production of photoinduce electrons in conduction band was also increased during this photocatalytic process.

Table 1 Kinetic parameters for the photocatalytic reduction of Cr(VI)

| Concentration of EDTA (ppm)	Rate constant (min^{-1})	$t_{1/2}$ (min)	R^2
0	1.6×10^{-2}	43	0.97
20	7.5×10^{-2}	9	0.99
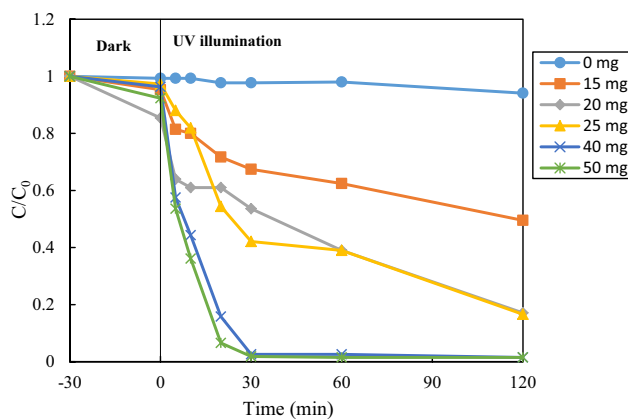
Fig. 2 Influence of ZnO dosage on the photocatalytic reduction of Cr(VI) in presence of 100 ppm EDTA

Eventually, the reduction efficiency of Cr(VI) would be enhanced greatly [38, 39].
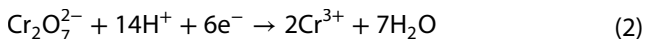
3.1.3 Influence of pH

The influence of pH on the photocatalytic reduction is addressed as an important parameter during photocatalytic treatment. The influence of pH was examined with various pH values from 3 to 10 with 40 mg ZnO and 20 ppm EDTA. It is observed in Fig. 3 that the photocatalytic Cr(VI) reduction was raised with declining the initial pH of solution. After 30 min of UV irradiation, the removal efficiency of Cr(VI) was 90%, 85.4%, 77.2%, 64% and 43% at pH = 3, 4, 6, 8 and 10, respectively. Therefore, the photocatalytic reduction of Cr(VI) occurred significantly at pH 3 rather than higher pH. This result can be illustrated by the relationships among surface charge of ZnO photocatalyst, pH values and speciation of Cr(VI) in solution [40]. Normally, chromium (VI) species exist as chromate (CrO_4^{2-}), dichromate ($Cr_2O_7^{2-}$), hydrogen chromate ($HCrO_4^-$),
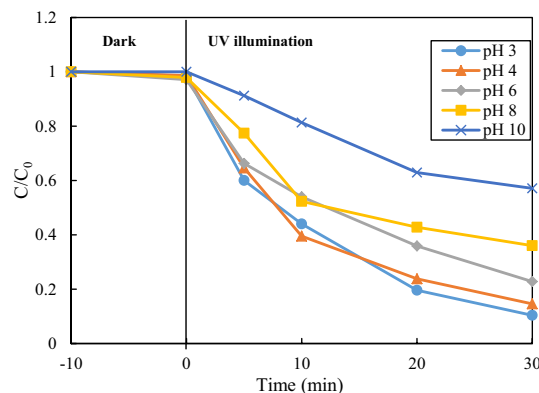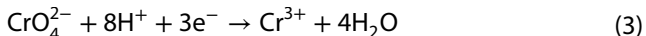

Fig. 3 Influence of pH on the photocatalytic reduction of Cr(VI) with 20 ppm EDTA

dihydrogen chromate (chromic acid, H_2CrO_4), hydrogen dichromate ($HCr_2O_7^-$), trichromate ($Cr_3O_{10}^{2-}$) and tetrachromate ($Cr_4O_{13}^{2-}$), where species depends on solution pH. The last three ions ($HCr_2O_7^-$, $Cr_3O_{10}^{2-}$ and $Cr_4O_{13}^{2-}$) have been observed only in solutions of pH < 0 or at a chromium (VI) concentration greater than 1 mol/L [41]. At low pH, Cr(VI) exists as $HCrO_4^-$ mainly, while CrO_4^{2-} occures at pH > 6.5 [25]. The pH_{pzc} of ZnO is 9 [42]. Hence, oxyanions of Cr(VI) can be readily absorbed on ZnO surface below the pH_{pzc} since ZnO surface becomes positively charged [43]. Moreover, the thermodynamic driving force between redox potential of Cr(VI)/Cr(III) and conduction band of photocatalyst became narrower with higher pH values as well as less photocatalytic reduction of Cr(VI) could be recorded [44]. The ZnO suface becomes negatively charged under alkaline condition which edges the conversion of $Cr_2O_7^{2-}$ oxyanions to CrO_4^{2-} ion as predominant species and lessens the reduction of Cr(VI). Again, $Cr(OH)_3$ can be deposited on the photocatalyst surface for decreasing its photocatalytic activity at higher pH [38]. Therefore, pH 3 was finalized as optimal pH for this reduction process. The photocatalytic reduction of Cr^{6+} ions to Cr^{3+} ions is presented depending on pH through Eqs. (2–4) [45].

At acidic condition:

$$Cr_2O_7^{2-} + 14H^+ + 6e^- \rightarrow 2Cr^{3+} + 7H_2O \qquad (2)$$

At neutral condition:

$$CrO_4^{2-} + 8H^+ + 3e^- \rightarrow Cr^{3+} + 4H_2O \qquad (3)$$

and at alkaline condition:

$$CrO_4^{2-} + 4H_2O + 3e^- \rightarrow Cr(OH)_3 + 5OH^- \qquad (4)$$
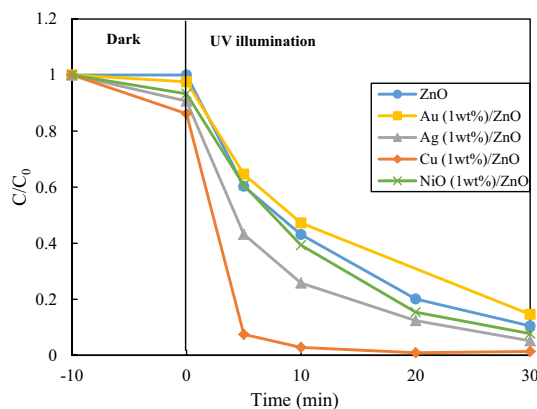
3.1.4 Influence of co-catalyst

A promising method to improve the photocatalytic activity of semiconductor–based photocatalysts is the loading of metal onto semiconductor materials. Thusly, Au, Ag, Cu and NiO were loaded on ZnO photocatalyst during photocatalytic reduction of Cr(VI) to scrutinize the effect of co-catalysts. Here, standard solution of Au, Ag and Cu ions, with given concentrations, were added directly into reaction solution while NiO particles were added by suspension method. The result is shown in Fig. 4. All of the 1 wt% metal modified ZnO resulted higher photocatalytic reduction of Cr(VI) compared with alone ZnO in presence of 20 ppm EDTA. Under UV irradiation, metal ions could trap the excited electrons in conduction band of ZnO photocatalyst and metal ions was reduced to metal and metal oxide which were deposited onto photocatalyst surface. Metal and metal oxide could help to retard the photoinduced electron–hole pair recombination [46]. Therefore, photocatalytic reduction of Cr(VI) was accelerated by 1 wt% metal doped ZnO nanoparticles.
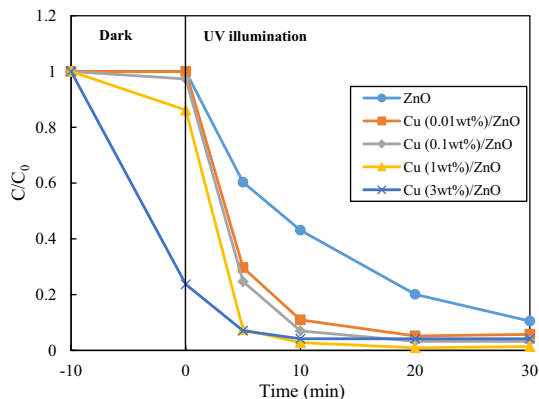
Fig. 4 Influence of co-catalyst on the reduction of Cr(VI) with ZnO in the presence of EDTA (20 ppm). Additives: Au 10 ppm (1 wt%), Ag 10 ppm (1 wt%), Cu 10 ppm (1 wt%) and NiO 10 ppm (1 wt%)

However, the reduction rate varies insignificantly in the order of Cu > Ag > NiO > Au. Although the similar mechanism could be observed for all these metals, photocatalytic activity varied slightly due to metal-catalytic properties. Copper ion could be reduced to both copper metal and Cu_2O by using conduction band electrons of photocatalyst. Cu metal and oxide trapped electron and stopped the electron–hole recombination. Moreover, Cu_2O released the electron and converted into CuO. These electrons could aslo reduce Cr(VI) to Cr(III). Therefore, photocatalytic reduction of Cr(VI) with Cu motivated ZnO was slightly more than other metals.

3.1.5 Influence of Cu amount

Cu was selected as co-catalyst with ZnO during the photocatalytic reduction of Cr(VI) since the photoreduction efficiency with Cu was quite higher compared to other co-catalysts. The effect of concentration of Cu on the photocatalytic Cr(VI) reduction was also studied and explained in Fig. 5. Although the adsorption of Cr(VI) on ZnO with different concentrations of Cu^{2+} ion were dissimilar in dark, the reduction efficiency with all concentration of Cu^{2+} ion were almost the same after 30 min irradiation. The sequence of reduction efficiency is 0 wt% < 0.01 wt% < 0.1 wt% < 3 wt% < 1 wt%. Hence, 1 wt% Cu accelerated the photocatalytic reduction compared with other concentration. The low doping of Cu may halt the electrons- holes recombination. On contrary, reaction rate can be adversely affected by high doping of Cu. For example, the deposited metallic copper could be oxidized to Cu^{2+} ions by consuming valence band holes for 3 wt% Cu doping [35].

Fig. 5 Influence of Cu doping amount on the reduction of Cr(VI) with ZnO in the presence of EDTA (20 ppm). Additives: Cu 0.1 ppm (0.01wt %), Cu 1 ppm (0.1 wt%) and Cu 10 ppm (1wt %)

3.2 Characterization of ZnO and Cu/ZnO photocatalysts

3.2.1 Textural characterization

The textural properties of ZnO and 1 wt% Cu/ZnO were examined by Brunauer–Emmett–Teller N_2 adsorption–desorption isotherm. The evaluation of the BET surface area and pore distribution of photocatalysts was shown in Fig. 6. As demonstrated in Fig. 6, the adsorption- desorption isotherm of ZnO and Cu/ZnO were confirmed the type IV isotherm, since the hysteresis loop was detected (Fig. 6a inset). The BET surface area, the total pore volume and the average pore diameter were presented in Table 2. All of parameters were increased due to the deposition of Cu with ZnO.

An image obtained by a transmission electron microscopy, is shown in Fig. 7 to study the morphology of ZnO and Cu/ZnO samples. It was clearly observed the nanoparticles were agglomerated and the shape was almost spherical with a hexagonal surface structure for pure ZnO. However, the morphology was considerably changed by

**Table 2** Textural properties of ZnO and 1wt % Cu/ZnO photocatalysts

|	Surface area (m^2/g)	Pore volume (cm^3/g)	Average pore diameter (nm)
ZnO	10.0	0.0374	15.0
Cu(1wt %)/ZnO	13.8	0.167	48.4

the doping of Cu. The small rod like structure of Cu/ZnO photocatalyst was detected. The Cu doping also suppressed the agglomeration of ZnO. Energy–dispersive X–ray spectroscopy (EDX) was performed for the elemental analysis of ZnO and Cu/ZnO photocatalysts. The electron mapping of Cu/ZnO nanoparticles are presented in Fig. S1 in Supplementary Material. As shown in Fig S1, the presence of Cu with ZnO could be confirmed.

3.2.2 XPS analysis

The chemical bonding state and the surface composition of Cu/ZnO photocatalyst was analyzed by XPS analysis. Figure 8 displays the XPS spectra of Cu/ZnO photocatalyst. The survey XPS spectrum is shown in Fig. 8a, demonstrating that the Zn 2p and Zn Auger peaks in addition to the Cu 2p, C 1s and O 1s peak. From Fig. 8b, the doublet spectral lines of Zn 2$p_{3/2}$ and 2$p_{1/2}$ due to spin–orbit coupling were recorded at the binding energy of 1021.94 eV and 1045.34 eV, respectively. These values were close to the standard ZnO binding energy values. According to this result, zinc(II) ion (Zn^{2+}) was confirmed in Cu/ZnO [3]. The O 1s spectra in Fig. 8c shows one peak located at 531.24 eV, which is attributed to lattice oxygen of ZnO photocatalyst. The high-resolution Cu 2p spectra are shown in Fig. 8d. The peak centered at 933.14 eV is attributed to Cu 2$p_{3/2}$, whereas the peak at 953.74 eV is ascribed to Cu 2$p_{1/2}$, indicating the existence of copper with the +2 oxidation state [47, 48].

Fig. 6 N_2 adsorption isotherms of ZnO (green) and 1wt % Cu/ZnO (orange) (**a**); pore size distribution curves of ZnO (green) and 1wt % Cu/ZnO (orange) (**b**)
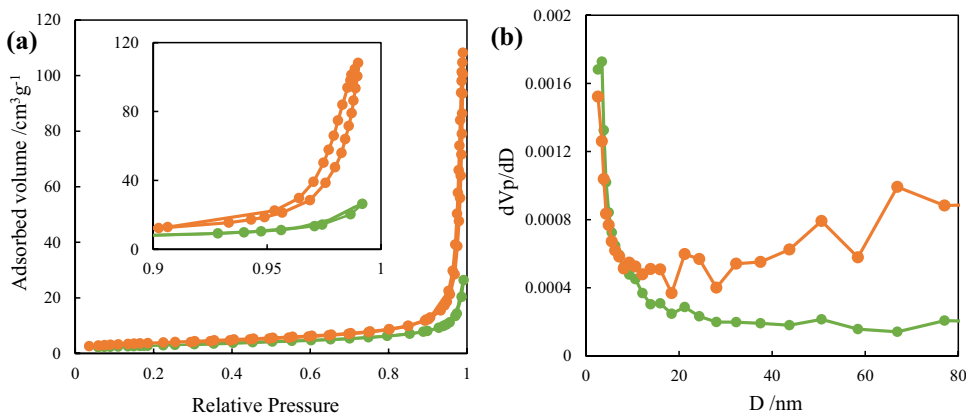
Fig. 7 TEM images of ZnO (**a**) and Cu/ZnO nanoparticles (**b**)
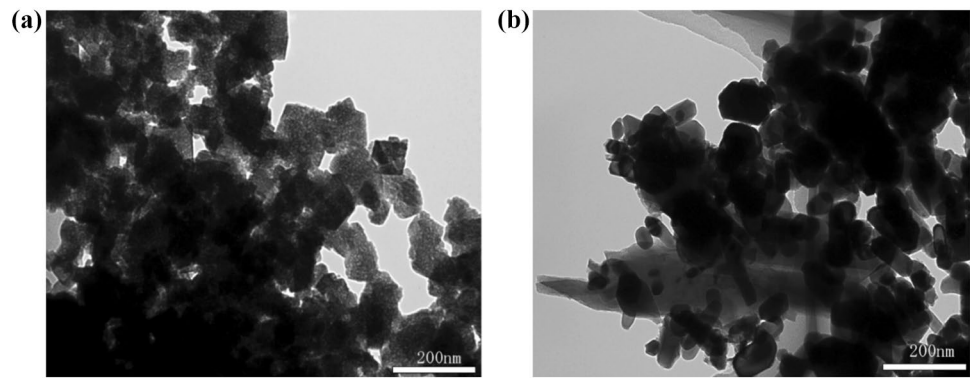
Fig. 8 High-resolution XPS spectra for 1 wt% Cu/ZnO nanoparticles. Survey spectra (**a**); Zn 2*p* (**b**); O 1*s* (**c**) and Cu 2*p* (**d**)
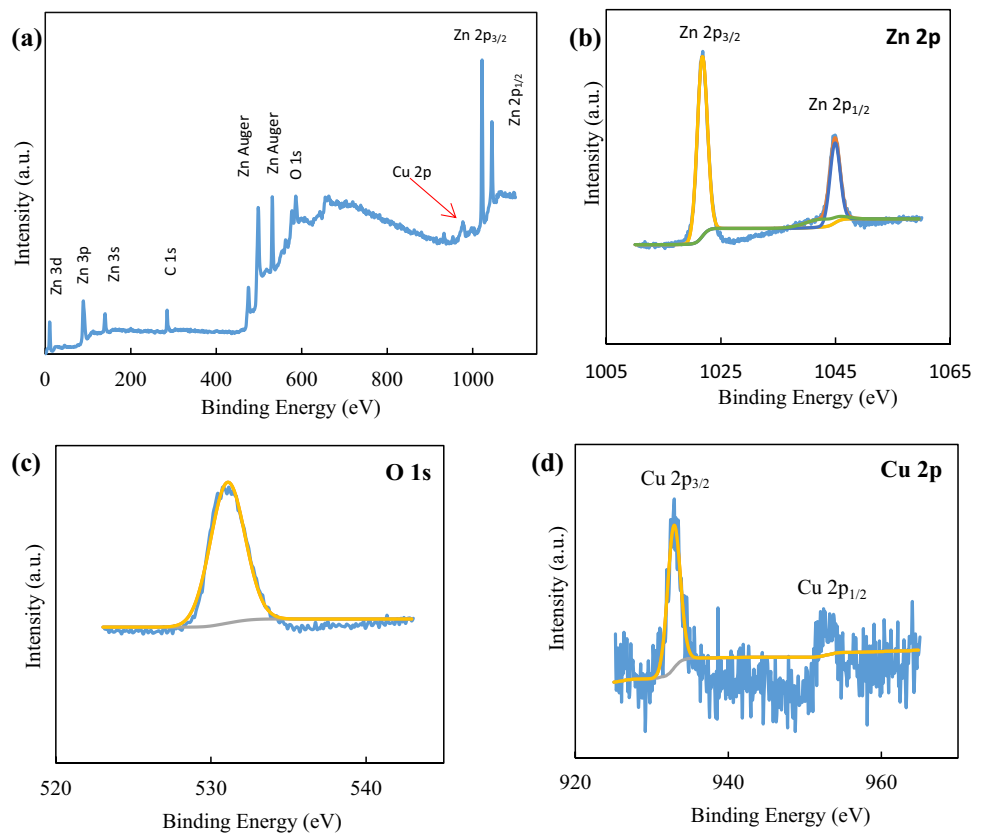
3.3 Optical properties

3.3.1 UV–Vis diffuse reflectance spectra

Figure 9 shows a comparison of the UV–Vis diffuse reflection spectrum of ZnO and 1 wt% Cu/ZnO. It was confirmed that Cu/ZnO exhibited a wide visible light absorbance in the range of 400–800 nm as well as the band absorbance of ZnO. The optical band gaps of ZnO and Cu/ZnO nanoparticles were calculated from the UV–Vis diffuse reflectance spectra (Fig. 9). The diffuse reflectance can be converted into absorption coefficient equivalent using Kubelka–Munk function, F(R), as represented below [49]

$$F(R) = (1 - R)^2/2R \tag{5}$$

where, F(R) is the Kubelka–Munk function of the sample and R is the reflectance of the sample. In the parabolic band structure, the Eg and absorption coefficient are related through the well-known Tauc relation [50]. The Tauc relation for a band gap material is given by the expression

$$\alpha h\nu = A(h\nu - E_g)^n \tag{6}$$

where, α is linear absorption coefficient, h is the Planck's constant, υ is light frequency, A is the proportionality constant and E_g is the band gap energy. The power of the

Fig. 9 UV–Vis diffuse reflectance spectra of ZnO and 1 wt% Cu/ZnO (**a**); Tauc plot of ZnO and 1 wt% Cu/ZnO (**b**)
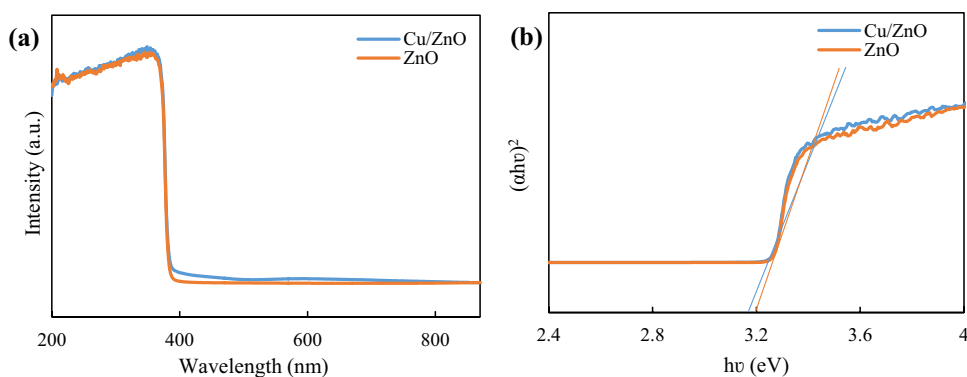
parenthesis is n = 2 or ½ for indirect and direct band gap materials, respectively. Because direct transition was found for ZnO, the direct band gap (Eg) could be obtained by plotting a graph of $(\alpha h\upsilon)^2$ against $h\upsilon$ based on the Tauc (Fig. 9b). By extrapolating the linear region of Tauc plot, the band gap of ZnO and 1 wt% Cu/ZnO were found to be 3.21 and 3.18 eV, respectively. The optical band bap of 1 wt% Cu/ZnO was slightly decreased as compared with that of pure ZnO.

3.3.2 Photoluminescence spectra

To elucidate the effect of Cu ion doping on the efficiency of charge–carrier trapping, immigration and transfer, the photoluminescence emission spectra of ZnO and 1 wt% Cu/ZnO with excitation source ranges from 325 to 350 nm are displayed in Fig. S2. Two peaks were detected in the PL spectra of pure ZnO nanoparticles in all of excitation sources. The peak found at about 398 nm in the ultraviolet region may be owing to the recombination of free exciton in the near–band–edge of ZnO. The other peak about 496 nm which exhibited a broad visible emission was generally attributed to the oxygen vacancies in ZnO lattices. Photoluminescence is evidently related with the recombination of the electron–hole pairs. The lower PL intensity confirms the slower photo-generated electron–hole pair recombination showing the enhancement of photocatalytic activity. Here, the PL intensities of Cu/ZnO nanoparticles were significantly lower than that of pure ZnO nanoparticles in all of excitation sources, demonstrating that a better optical properties of Cu/ZnO. The fact could be ascribed to it that the Cu can trap several electrons to suppress the recombination of electron–hole pairs for 1 wt% Cu/ZnO photocatalyst. The comparison of PL intensities explained that Cu/ZnO had a lower recombination rate and better optical properties.

3.4 Cr(VI) Reduction mechanism

The mechanism of the photocatalytic reduction of Cr(VI) by 1 wt% Cu/ZnO in presence of EDTA is a very complicated reaction. However a plausible mechanism was presented in Scheme 1. The mechanism was based on three aspects, (1) the small amount of Cu could be acted as electron trapping sites which reduced the electron–hole recombination gently; (2) the one step reduction of Cr(VI) to Cr(III) by the photo–generated electrons (e⁻); (3) water was oxidized by valence band holes to produce highly active hydroxyl radicals, therefore, sacrificial electron donor (EDTA) could be oxidized by both valence band holes and hydroxyl radicals.

The conduction band and valence band of ZnO are positioned at − 3.9 eV and − 7.1 eV (vs. AVS), respectively [51]. The estimated band gap of 1 wt% Cu/ZnO was 3.18 eV (Fig. 9). Under UV irradiation, the Cu/ZnO (bandgap of 3.18 eV) absorbed the photons efficiently and was excited to form electrons in the conduction band (CB) and holes in the valance band (VB). Theoretically, Cu^{2+} ions are reduced to Cu metal and Cu_2O, which are deposited on ZnO surface in solution under UV irradiation [52]. The standard reduction potential of Cu^{2+}/Cu and Cu^{2+}/Cu^+ are + 0.35 V and + 0.15 V versus NHE, respectively [53,
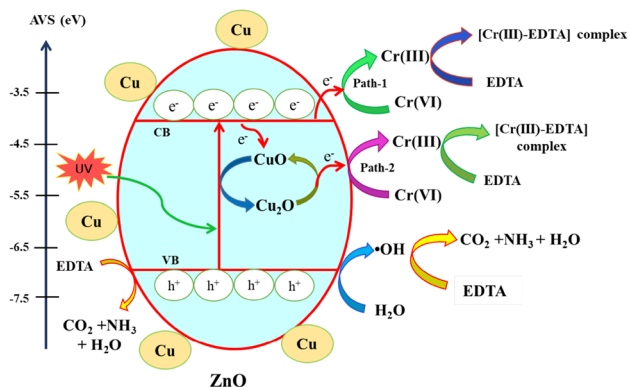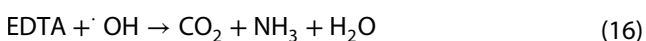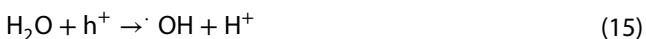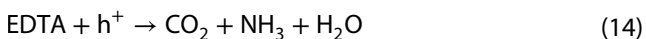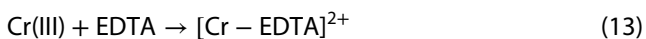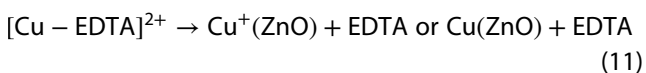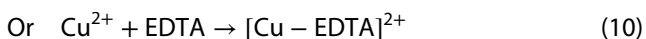

**Scheme 1** Proposed mechanism for photocatalytic Cr(VI) reduction with 1 wt% Cu/ZnO in presence of EDTA under UV illumination

54]. Hence, reduction of Cu^{2+} ion to metallic Cu and Cu^+ ion are thermodynamically possible by photogenerated electron of less negative ZnO conduction band potential. Here, Cu^+ ions were quickly converted into Cu_2O, since Cu^+ ions were quite unstable. The released electron from Cu_2O could reduce Cr(VI) to Cr(III). In addition, the Cr(VI)/Cr(III) redox couple has a more positive reduction potential, $E^0(HCrO_4^-/Cr^{3+}) = +1.35$ V versus NHE [55] with respect to ZnO conduction band edge. Therefore, the originated conduction band electrons reduce Cr(VI) to Cr(III) thermodynamically. EDTA has been applied to enhance the photocatalytic Cr(VI) reduction with Cu/ZnO. The complex of EDTA with reduced Cr(III), $[Cr-(EDTA)]^{3+}$ as final product of this reduction process. $[Cr-(EDTA)]^{3+}$ complex is soluble and cannot occur on ZnO surface. Therefore, reduction process was benefited.

The point of zero charge (pzc) of the ZnO particle is approximately 9. When the pH is lower than this value, the ZnO surface becomes positively charged. From the estimation of Cr(VI) species as the function of pH, the main chemical species for hexavalent chromium at pH 3 is $HCrO_4^-$. Owing to the electrostatic attraction between $HCrO_4^-$ species and ZnO photocatalyst with a relatively large surface area, as well as the facilitation of the proton under acidic conditions, adsorbed Cr(VI) on the surface of ZnO can be immediately reacted with electrons and be reduced to Cr(III). The reaction related in this photoreduction process are represented in Eqs. (7–16).

$$ZnO + h\nu \rightarrow e^- + h^+ \tag{7}$$

$$Cu^{2+} + e^- \rightarrow Cu^+ \tag{8}$$

$$Cu^+ \rightarrow Cu^{2+} + e^- \tag{9}$$

$$Or \quad Cu^{2+} + EDTA \rightarrow [Cu-EDTA]^{2+} \tag{10}$$

$$[Cu-EDTA]^{2+} \rightarrow Cu^+(ZnO) + EDTA \text{ or } Cu(ZnO) + EDTA \tag{11}$$

$$Cr(VI) + 3e^- \rightarrow Cr(III) \tag{12}$$

$$Cr(III) + EDTA \rightarrow [Cr-EDTA]^{2+} \tag{13}$$

$$EDTA + h^+ \rightarrow CO_2 + NH_3 + H_2O \tag{14}$$

$$H_2O + h^+ \rightarrow \cdot OH + H^+ \tag{15}$$

$$EDTA + \cdot OH \rightarrow CO_2 + NH_3 + H_2O \tag{16}$$

The deactivation of photocatalyst surface, due to adsorption of Cr(III) species, could be prevented by the formation of $[Cr-EDTA]^{3+}$ complex in reaction solution [36, 56]. Simultaneously, EDTA could consume valence band holes (h^+) directly, and EDTA was oxidized by hydroxyl radical. EDTA was converted to carbon dioxide, ammonia and
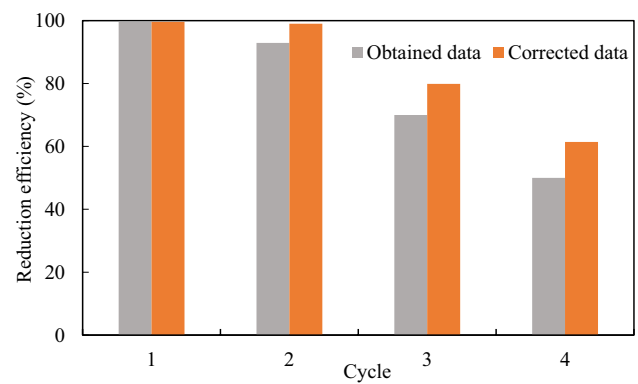
Fig. 10 Reusability of 1 wt% Cu/ZnO for the reduction of Cr(VI)

water after several steps. Thus, EDTA played duel role during this reduction process. As a result, the recombination of electrons and holes was suppressed favoring the fast photocatalytic Cr(VI) reduction.

3.5 Reusability

The reusability of 1 wt% Cu/ZnO was investigated by conducting the circulating runs in the photocatalytic Cr(VI) reduction under UV illumination. The reaction solution was separated after completing one cycle, therefore, a certain amount of photocatalyst could be lost after every cycle. Hence, the obtained reduction efficiency should be corrected, taking account of the decreased amount of photocatalyst in the reaction solution. As shown in Fig. 10, the photocatalytic activity of Cu/ZnO was decreased slowly with every cycles and after fourth cycles about 60% of reduction efficiency was recorded.

4 Conclusion

In summary, this research work aids a procedure to enrich the photocatalytic activity of ZnO nanoparticles with 1 wt% Cu doping in presence of ethylene diaminetetraacetic acid (EDTA) to reduce Cr(VI) to Cr(III). The effect of factors revealed that the small particle size of ZnO, low pH value (pH > 3), the proper amount EDTA and Cu doping and ZnO, photocatalyst dosage could promote the reduction of Cr(VI). The highest 98.5% of reduction of Cr(VI) was recorded with 20 ppm EDTA after only 120 min. Increasing the photocatalyst dosages resulted the significant improvement in the reduction of Cr(VI). Similarly, photocatalytic reduction of Cr(VI) led to decreasing from 90 to 43% as initial pH increased 3 to 10 after 30 min UV irradiation. Briefly, Cu doping retarded the photoinduced electron–hole recombination while EDTA immensely influenced this photocatalytic Cr(VI) reduction process by removing of Cr(III) from ZnO photocatalyst surface

and capturing holes of valence band. These two factors could simultaneously provide a sovereign way for the efficient removal of Cr(VI) under UV irradiation. Therefore, the present treatment method is simple, low cost and easy–handling.

Compliance with ethical standards

Conflict of interest The authors declare no conflict of interest.

References

1. Korak JA, Huggins R, Arias-Paic P (2017) Regeneration of pilot-scale ion exchange columns for hexavalent chromium removal. Water Res 118:141–151. https://doi.org/10.1016/j.watres.2017.03.018

2. Du XD, Yi XH, Wang P, Zheng W, Deng J, Wang CC (2019) Robust photocatalytic reduction of Cr(VI) on UiO-66-NH2(Zr/Hf) metal-organic framework membrane under sunlight irradiation. Chem Eng J 356:393–399. https://doi.org/10.1016/j.cej.2018.09.084

3. Bao C, Chen M, Jin X, Hu D, Huang Q (2019) Efficient and stable photocatalytic reduction of aqueous hexavalent chromium ions by polyaniline surface-hybridized ZnO nanosheets. J Mol Liq 279:133–145. https://doi.org/10.1016/j.molliq.2019.01.122

4. Bakshi A, Panigrahi AK (2018) A comprehensive review on chromium induced alterations in fresh water fishes. Toxicol Rep 5:440–447. https://doi.org/10.1016/j.toxrep.2018.03.007

5. Shahid M, Shamshad S, Rafiq M, Khalid S, Bibi I, Niazi NK, Dumat C, Rashid MI (2017) Chromium speciation, bioavailability, uptake, toxicity and detoxification in soil-plant system: a review. Chemosphere 178:513–533. https://doi.org/10.1016/j.chemosphere.2017.03.074

6. Li J, Liu Z, Zhu Z (2015) Enhanced photocatalytic activity of $ZnFe_2O_4$–ZnO–Ag_3O_4 hollow nanospheres through the cascadal electron transfer with magnetical separation. J Alloys Compd 636:229–233. https://doi.org/10.1016/j.jallcom.2015.02.176

7. Samadi MT, Saghi MH, Rahmani A, Rahimi S, Syboney MS (2010) Hamadan landfill leachate treatment by coagulation-flocculation process. Iran J Environ Health Sci Eng 7(3):253–258

8. Siboni MS, Khataee A, Vafaei F, Joo SW (2014) Comparative removal of two textile dyes from aqueous solution by adsorption onto marine-source waste shell: kinetic and isotherm studies. Korean J Chem Eng 31(8):1451–1459. https://doi.org/10.1007/s11814-014-0085-4

9. Siboni MS, Jafari S-J, Farrokhi M, Yang JK (2013) Removal of phenol from aqueous solutions by activated red mud: equilibrium and kinetics studies. Environ Eng Res 18(4):247–252. https://doi.org/10.4491/eer.2013.18.4.247

10. Natale FD, Erto A, Lancia A, Musmarra D (2015) Equilibrium and dynamic study on hexavalent chromium adsorption onto activated carbon. J Hazard Mater 281:47–55. https://doi.org/10.1016/j.jhazmat.2014.07.072

11. Qi H, Wang S, Liu H, Gao Y, Wang T, Huang Y (2016) Synthesis of an organic–inorganic polypyrrole/titanium(IV) biphosphate hybrid for Cr(VI) removal. J Mol Liq 215:402–409. https://doi.org/10.1016/j.molliq.2015.12.060

12. Mohagheghian A, Karimi SA, Yang JK, Siboni MS (2015) Photocatalytic degradation of a textile dye by illuminated tungsten oxide nanopowder. J Adv Oxid Technol 18(1):61–68. https://doi.org/10.1515/jaots-2015-0108

13. Saien J, Azizi A, Soleymani AR (2014) Parameter evaluation, kinetics, and energy consumption for Cr(VI) photocatalytic reduction under mild conditions. J Iran Chem Soc 11:1439–1448. https://doi.org/10.1007/s13738-014-0419-5

14. Yan X, Ning G, Zhao P (2019) Enhanced visible light photocatalytic reduction of Cr(VI) over a novel square nanotube poly(triazine amide)/TiO_2 heterojunction. Catalysts 9:55–66. https://doi.org/10.3390/catal9010055

15. Ravishankar TN, Vaz MO, Ramakrishnappa T, Teixeira SR, Dupont J (2017) Ionic liquid assisted hydrothermal syntheses of Au doped TiO_2 NPs for efficient visible-light photocatalytic hydrogen production from water, electrochemical detection and photochemical detoxification of hexavalent chromium (Cr^{6+}). RSC Adv 7:43233–43244. https://doi.org/10.1039/C7RA04944G

16. Ibhadon AO, Fitzpatrick P (2013) Heterogeneous photocatalysis: recent advances and applications. Catalysts 3(1):189–218. https://doi.org/10.3390/catal3010189

17. Siboni MS, Samarghandi MR, Yang JK, Lee SM (2011) Photocatalytic removal of cyanide with illuminated TiO_2. Wat Sci Tech. 64(7):1383–1387. https://doi.org/10.2166/wst.2011.738

18. Mohagheghian A, Karimi SA, Yang JK, Siboni MS (2016) Photocatalytic degradation of diazinon by illuminated WO_3 nanopowder. Desalin Water Treat 57(18):8262–8269. https://doi.org/10.1080/19443994.2015.1017009

19. Mohagheghian A, Pourmohseni M, Vahidi-Kolur R, Yang JK, Siboni MS (2017) Application of kaolin–Fe_3O_4 nano-composite for the removal of azo dye from aqueous solutions. Desalin Water Treat 58:308–319. https://doi.org/10.5004/dwt.2017.0198

20. Humayun M, Raziq F, Khan A, Luo W (2018) Modification strategies of TiO_2 for potential applications in photocatalysis: a critical review. Green Chem Lett Rev 11(2):86–102. https://doi.org/10.1080/17518253.2018.1440324

21. Guo Q, Zhou C, Ma Z, Ren Z, Fan H, Yang X (2016) Elementary photocatalytic chemistry on TiO_2 surfaces. Chem Soc Rev 45:3701–3730. https://doi.org/10.1039/C5CS00448A

22. Siboni MS, Khataee A, Vahid B, Joo SW (2015) Synthesis, characterization and immobilization of ZnO nanosheets on scallop shell for photocatalytic degradation of an insecticide. Sci Adv 7(4):806–814. https://doi.org/10.1166/sam.2015.2163

23. Siboni MS, Khataee A, Vahid B, Joo SW, Fallah S (2014) Preparation of a green photocatalyst by immobilization of synthesized ZnO nanosheets on scallop shell for degradation of an azo dye. Curr Nanosci 10(5):684–694. https://doi.org/10.2174/1573413713710666140521175816

24. Chu DW, Masuda Y, Ohji T, Kato K (2010) Formation and photocatalytic application of ZnO nanotubes using aqueous solution. Langmuir 26:2811–2815. https://doi.org/10.1021/la902866a

25. Islam JB, Furukawa M, Tateshi I, Katsumata H, Kaneco S (2019) Photocatalytic reduction of hexavalent chromium with nanosized TiO_2 in presence of formic acid. ChemEngineering 3:33–42. https://doi.org/10.3390/chemengineering3020033

26. Rameshbabu R, Kumar N, Karthigeyan A, Neppolian B (2016) Visible light photocatalytic activities of $ZnFe_2O_4$/ZnO nanoparticles for the degradation of organic pollutants. Mater Chem Phys 18:106–115. https://doi.org/10.1016/j.matchemphys.2016.06.040

27. Gholami M, Siboni MS, Farzadkia M, Yang JK (2016) Synthesis, characterization, and application of ZnO/TiO_2 nanocomposite for photocatalysis of a herbicide (Bentazon). Desalin Water Treat 57(29):13632–13644. https://doi.org/10.1080/19443994.2015.1060541

28. Siboni MS, Jonidi-Jafari A, Farzadkia M, Esrafili A, Gholami M (2017) Enhancement of photocatalytic activity of Cu-doped ZnO nanorods for the degradation of an insecticide: kinetics and reaction pathways. J Environ Manage 186:1–11. https://doi.org/10.1016/j.jenvman.2016.10.049

29. Gholami M, Siboni MS, Yang JK (2016) Application of Ni-doped ZnO rods for the degradation of an azo dye from aqueous solutions. Korean J Chem Eng 33(3):812–882. https://doi.org/10.1007/s11814-015-0218-4

30. Samarghandi MR, Yang JK, Lee SM, Giahi O, Siboni MS (2014) Effect of different type of organic compounds on the photocatalytic reduction of Cr(VI) in presence of ZnO nanoparticles. Desalin Water Treat 52(7–9):1531–1538. https://doi.org/10.1080/19443994.2013.797624

31. Babay PA, Emilio CA, Ferreyra RE, Gautier EA, Gettar RT, Litter MI (2001) Kinetics and mechanisms of EDTA photocatalytic degradation with TiO₂. Wat Sci Tech 44(5):179–185. https://doi.org/10.2166/wst.2001.0281

32. Westin KJ, Rasmuso ÅC (2005) Nucleation of calcium carbonate in presence of citric acid, DTPA, EDTA and pyromellitic acid. J Colloid Interf Sci 282:370–379. https://doi.org/10.1016/j.jcis.2004.09.071

33. Siemon U, Bahnemann D, Testa JJ, Rodríguez D, Litter MI, Bruno N (2002) Heterogeneous photocatalytic reactions comparing TiO₂ and Pt/TiO₂. J Photochem Photobiol, A 148:247–255. https://doi.org/10.1016/S1010-6030(02)00050-3

34. Bhanushali S, Ghosh P, Ganesh A, Cheng WL (2015) 1D copper nanostructures: progress, challenges and opportunities. Small 11:1232–1252. https://doi.org/10.1002/smll.201402295

35. Janczarek M, Kowalska E (2017) On the origin of enhanced photocatalytic activity of copper-modified titania in the oxidative reaction systems. Catalysts 7:317–343. https://doi.org/10.3390/catal7110317

36. Meichtry JM, Colbeau-Justin C, Custo G, Litter MI (2014) Preservation of the photocatalytic activity of TiO₂ by EDTA in the reductive transformation of Cr(VI). Studies by time resolved microwave conductivity. Catal Today 224:236–243. https://doi.org/10.1016/j.cattod.2013.10.021

37. Sofi FA, Majid K, Mehraj O (2018) The visible light driven copper based metal-organic-framework heterojunction:HKUST-1@Ag–Ag₃PO₄ for plasmon enhanced visible light photocatalysis. J Alloys Compd 737:798–808. https://doi.org/10.1016/j.jallcom.2017.12.141

38. Shao D, Wang X, Fan Q (2009) Photocatalytic reduction of Cr(VI) to Cr(III) in solution containing ZnO or ZSM-5 zeolite using oxalate as model organic compound in environment. Microporous Mesoporous Mater 117:243–248. https://doi.org/10.1016/j.micromeso.2008.06.026

39. Ku Y, Jung IL (2001) Photocatalytic reduction of Cr(VI) in aqueous solutions by UV irradiation with the presence of titanium dioxide. Water Res 35:135–142. https://doi.org/10.1016/S0043-1354(00)00098-1

40. Xu Q, Li R, Wang C, Yuan D (2017) Visible-light photocatalytic reduction of Cr(VI) using nano-sized delafossite (CuFeO₂) synthesized by hydrothermal method. J Alloys Compd 723:441–447. https://doi.org/10.1016/j.jallcom.2017.06.243

41. Szabó M, Kalmár J, Ditrói T, Bellér G, Lente G, Simic N, Fábián I (2018) Equilibria and kinetics of chromium(VI) speciation in aqueous solution—a comprehensive study from pH 2 to 11. Inorg Chim Acta 472:295–301. https://doi.org/10.1016/j.ica.2017.05.038

42. Naimi-Joubani M, Shirzad MS, Yang JK, Gholami M, Farzadkia M (2015) Photocatalytic reduction of hexavalent chromium with illuminated ZnO/TiO₂ composite. J Ind Eng Chem 22:317–323. https://doi.org/10.1016/j.jiec.2014.07.025

43. Liu SX (2005) Removal of copper (VI) from aqueous solution by Ag/TiO₂ photocatalysis. Bull Environ Contam Toxicol 74:706–714. https://doi.org/10.1007/s00128-005-0640-0

44. Wang N, Zhu L, Deng K, She Y, Yu Y, Tang H (2010) Visible light photocatalytic reduction of Cr(VI) on TiO₂ on situ modified with the small molecular weight organic acids. Appl Catal B-Environ 95(3–4):400–407. https://doi.org/10.1016/j.apcatb.2010.01.019

45. Shirzad MS, Samadi MT, Yang JK, Lee SM (2012) Photocatalytic removal of Cr(VI) and Ni(II) by UV/TiO₂: kinetic study. Desalin Wat Treat 40:77–83. https://doi.org/10.1080/19443994.2012.671144

46. Wu SX, Ma Z, Qin YN, He F, Jia LS, Zhang YJ (2003) XPS study of copper doping TiO₂ photocatalyst. Acta Phys Chim Sin 19:967–969. https://doi.org/10.3866/PKU.WHXB20031017

47. Pashchanka M, Hoffmann RC, Gurlo A, Swarbrick JC, Khanderi J, Engstler J, Issanin A, Schneider JJ (2011) A molecular approach to Cu doped ZnO nanorods with tunable dopant content. Dalton Trans 40:4307–4314. https://doi.org/10.1039/c0dt01567a

48. Pung S, Ong C, Isha KM, Othman M (2014) Synthesis and characterization of Cu-doped ZnO nanorods. Sains Malays 43:273–281

49. Das TK, Illaiyaraja P, Mocherla PSV, Bhalerao GM (2016) Influence of surface disorder, oxygen defects and bandgap in TiO₂ nanostructures on the photovoltaic properties of dye sensitized solar cells. Sol Energy Mater Sol Cells 144:194–209. https://doi.org/10.1016/j.solmat.2015.08.036

50. Valenzuela MA, Bosch P, Jiménez-Becerrill J, Quiroz O, Páez AI (2002) Preparation, characterization and photocatalytic activity of ZnO, Fe₂O₃ and ZnFe₂O₄. J Photochem Photobiol, A 148:177–182. https://doi.org/10.1016/S1010-6030(02)00040-0

51. Tahir M, Tahir B, Amina NAS, Alias H (2016) Selective photocatalytic reduction of CO₂ by H₂O/H₂ to CH₄ and CH₃OH over Cu-promoted In₂O₃/TiO₂ nanocatalyst. Appl Surf Sci 389:46–55. https://doi.org/10.1016/j.apsusc.2016.06.155

52. Jacobs JWM, Kampers FWH, Rikken JMG, Bulle-Lieuwma CWT, Koningsberger DC (1989) Copper photodeposition on titanium dioxide studied with HREM and EXAFS. J Electrochem Soc 136:2914–2923. https://doi.org/10.1149/1.2096373

53. Sykora J (1997) Photochemistry of copper complexes and their environmental aspects. Coord Chem Rev 159:95–105. https://doi.org/10.1016/S0010-8545(96)01299-4

54. Wang L, Lia X, Teng W, Zhao Q, Shi Y, Yue R, Chen Y (2013) Efficient photocatalytic reduction of aqueous Cr(VI) over flower-like SnIn₄S₈ microspheres under visible light illumination. J Hazard Mater 244–245:681–688. https://doi.org/10.1016/j.jhazmat.2012.10.062

55. Zhu J, Shao C, Li X, Han C, Yang S, Ma J, Li X, Liu Y (2018) Immobilization of ZnO/polyaniline heterojunction on electrospun polyacrylonitrile nanofibers and enhanced photocatalytic activity. Mater Chem Phys 214:507–515. https://doi.org/10.1016/j.matchemphys.2018.04.053

56. Choi Y, Koo MS, Bokare AD, Kim D, Bahnemann DW, Choi W (2017) Sequential process combination of photocatalytic oxidation and dark reduction for the removal of organic pollutants and Cr(VI) using Ag/TiO₂. Environ Sci Technol 51:3973–3981. https://doi.org/10.1021/acs.est.6b06303